

Structural Characterization of Lanthanum Chromite Perovskite Coating Deposited by Magnetron Sputtering on an Iron-Based Chromium-Containing Alloy as a Promising Interconnect Material for SOFCs

Nina Orlovskaya* and Anthony Coratolo

Department of Materials Engineering, Drexel University, Philadelphia, Pennsylvania 19104

Christopher Johnson and Randall Gemmen

Department of Energy, National Energy Technology Laboratory, Morgantown, West Virginia 26507

Chromium-containing stainless steel (SS) is a prospective material for use as an interconnect in solid oxide fuel cells (SOFCs). However, during operations at high temperatures, the growth of oxide scales causes the performance of the interconnect and SOFC as a whole to deteriorate. The coating of SS 446 with a conducting perovskite is a potential method of slowing the growth of oxide scale and, therefore, improving overall SOFC performance. In the present research, the structural characterization of a pure LaCrO_3 thin film on the SS 446 substrates has been performed as a model material that can be used as a barrier coating for the metallic interconnect. The deposition of an amorphous La-Cr-O thin film on SS 446 was performed using radio-frequency (rf) magnetron sputtering. The deposited amorphous film was annealed in air to form the desired perovskite phase. The film underwent an amorphous to LaCrO_4 phase transition during annealing at 500°C with further transformation to LaCrO_3 orthorhombic phase during annealing at 700°C . A self-organized dendritic structure was reported as a result of the perovskite-phase formation. Although formation of various oxides, such as Fe_2O_3 and Fe_3O_4 , was observed during the annealing of uncoated SS 446 in air, the coating of SS 446 surface with LaCrO_3 film prevented formation of various oxide phases at the interconnect surface. The structural characterization of the films and SS 446 surfaces was accomplished using scanning electron microscopy with energy-dispersive X-ray analysis, X-ray diffractometry, micro-Raman spectroscopy, and nanoindentation.

I. Introduction

MATERIALS used as interconnects in solid oxide fuel cells (SOFCs) must meet several requirements.¹ The material must be electronically conducting (low ionic conductivity), be gas impervious, have a coefficient of thermal expansion (CTE) match to other SOFC components, be stable under oxidizing and reducing atmospheres, and have low creep, sufficient strength, and good thermal conductivity. When SOFCs operated at temperatures near 1000°C , the leading candidate material for

the interconnect application was lanthanum chromite (LaCrO_3). LaCrO_3 -based perovskite ceramics meet several of the requirements listed above, but are brittle and expensive to process. The recent lowering of the typical operating temperatures for SOFCs from 1000° to $<800^\circ\text{C}$ has led to the proposed use of less-expensive chromium-containing alloys as interconnects and current collectors in SOFC systems.^{2,3}

The chromium-containing alloys are superior in most respects to their ceramic counterparts. They have good strength, electrical conductivity, and low cost. The chromium-containing alloys are chosen over other high-temperature alloys because of the relatively good electrical conductivity of the chromia (Cr_2O_3) scale. Problems persist, however, with regard to the long-term use of these alloys. At operating temperature, the oxide layer grows thicker over time and, therefore, resistance gradually increases. As the layer grows thicker, it also has a tendency to lose adhesion to the underlying metals. At high temperatures, chromium also can migrate and contaminate other cell components, which affects the total cell/stack performance.

Several methods of mitigating the problems associated with using chromium-containing alloys as interconnect materials have been studied. It has been found that the addition of thin layers of surface dopants,^{4,5} such as yttrium, lanthanum, and cerium can change the growth mechanism of the oxide scale, which effectively improves the adhesion of oxide and slows the rate of growth. Another approach is to allow the interfacial oxide layer to grow but to dope the surface with another material that decreases the area specific resistance of the Cr_2O_3 scale.^{6,7} Yet another approach is to coat the interconnect with a conducting oxide layer, such as an electrically conductive perovskite, to suppress oxidation of the chromium-containing stainless steel (SS).^{8,9} It is important that the protective layer be as dense as possible to maximize the effectiveness of such coatings. Coating with perovskites also may be advantageous from the standpoint of targeted control over the protective layer properties. Perovskites, such as LaCrO_3 , can be easily doped on the A or B sites to adjust important properties, such as conductivity¹⁰ and CTE,¹¹ to be more compatible with the interconnect material.

The deposition of perovskite thin films can be accomplished by a variety of techniques, among them sol-gel coating,¹² laser ablation,¹³ pulsed laser deposition,¹⁴ electrostatic spray deposition,¹⁵ and sputter deposition.^{16,17} Here, we report results on the characterization of a radio-frequency (rf) magnetron-sputtered LaCrO_3 perovskite film on SS as a potential method of improving the effectiveness of alloy interconnect functions. The pure LaCrO_3 thin film is used as a model material for a barrier coating for metallic interconnect.

N. J. Dudney—contributing editor

Manuscript No. 10032. Received March 10, 2003; approved May 27, 2004.
Work at Drexel University supported by the National Energy Technology Laboratory, U.S. Department of Energy, under Contract No. 239811.
*Member, American Ceramic Society.

II. Experimental Procedures

Thin films were deposited by rf magnetron sputtering on chromium-containing SS substrates. The magnetron sputtering was performed at Thin Films, Inc. Highly porous (40%) light-green-colored LaCrO_3 perovskite was used as a target material. The energy-dispersive spectroscopy (EDS) analysis of a target LaCrO_3 showed a slight excess of chromium with a La/Cr atomic ratio of 49.11/50.89. SS substrates (10 mm \times 10 mm \times 5 mm, SS 446) were polished using a diamond spray to a mirror surface. The substrates were coated in the rf sputtering mode under an 8×10^{-3} torr (1.1 Pa) argon-ion atmosphere. The substrate temperature was 25°C at the beginning of deposition. The target to substrate distance was 5 cm. After the target was presputtered for 30 min, the substrate was moved into position under the target and then remained stationary. The total time of sputter deposition, at 500 W of power, was 5 h. Film thickness, measured using an interferometric surface profiler (Phase Shift Technology, Tucson, AZ), was 2000 ± 200 Å. EDS of an as-received film composition resulted in a La/Cr atomic ratio of 56.54/43. After it was sputtered, the SS with deposited film was annealed at 300°, 500°, and 700°C for a certain period of time at a controlled heating rate of 30°C/min in air. For comparison, polished SS samples without a thin film were annealed for the same period of time. The cooling rate after dwelling at 300° and 500°C for 15 min was 20°C/min, whereas, after dwelling at 700°C for 1 h, the samples were taken out of the furnace and cooled in the air. After they were annealed at each temperature, X-ray diffraction (XRD) patterns and Raman spectra were acquired from LaCrO_3 deposited and polished SS samples.

A diffractometer (Siemens, Karlsruhe, Germany) was used to determine the crystal structure of the LaCrO_3 films heated to

700°C. A micro-Raman spectrometer (Model 1000, Renishaw, New Mills, Gloucestershire, U.K.) was used to study the vibrational spectra of the film and substrate surfaces. The excitation light was a 514.5 nm line of an argon-ion laser. The incident and scattered beams were focused using a microscope with a 50 \times objective (Olympus Optical Co., Tokyo, Japan), which allowed a laser spot as small as 4–5 μm . All measurements were performed at room temperature. The Raman bands were deconvoluted using GRAMS software.

Nanoindentation tests were performed (Model XP, Nanoin-denter) on an as-deposited thin film.^{18,19} An indenter (Berkovich) was used to indent the film. Nanoindentation tests were performed in the displacement control mode with a maximum 300 nm displacement allowed. At least 10 indents were made for each test with significant distances between indents. The loading and unloading rates were the same in each experiment; however, the rate varied from 0.022 to 0.42 mN/s as the maximum displacement increased from 50 to 300 nm.

III. Results and Discussion

(1) Film Structure—Scanning Electron Microscopy

Scanning electron microscopy (SEM) images of the as-deposited films are shown in Figs. 1(a) and (b). The small dark regions that appear probably are the result of segregation during the sputtering process. Comparison using EDS analysis of the typical film surface and the dark regions is shown in Figs. 1(c) and (d). The EDS analysis shows that the small dark regions are enriched in chromium. EDS analysis also shows that oxygen content in the as-deposited film is less than stoichiometric.

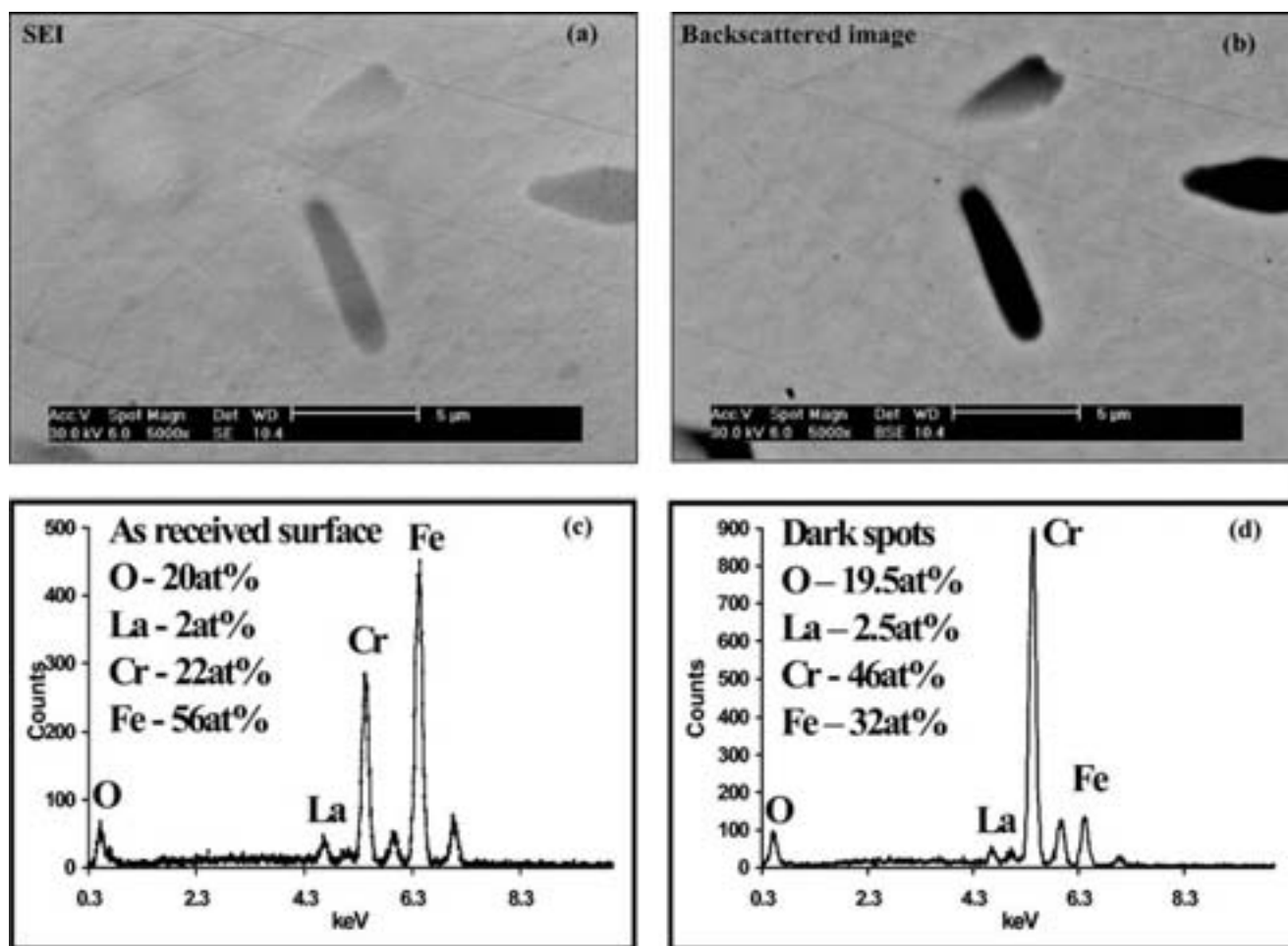


Fig. 1. La-Cr-O surface after magnetron sputtering: (a) secondary electron image (SEI); (b) backscattered image; (c) EDS analysis of the as-received surface; and (d) EDS analysis of the dark spot.

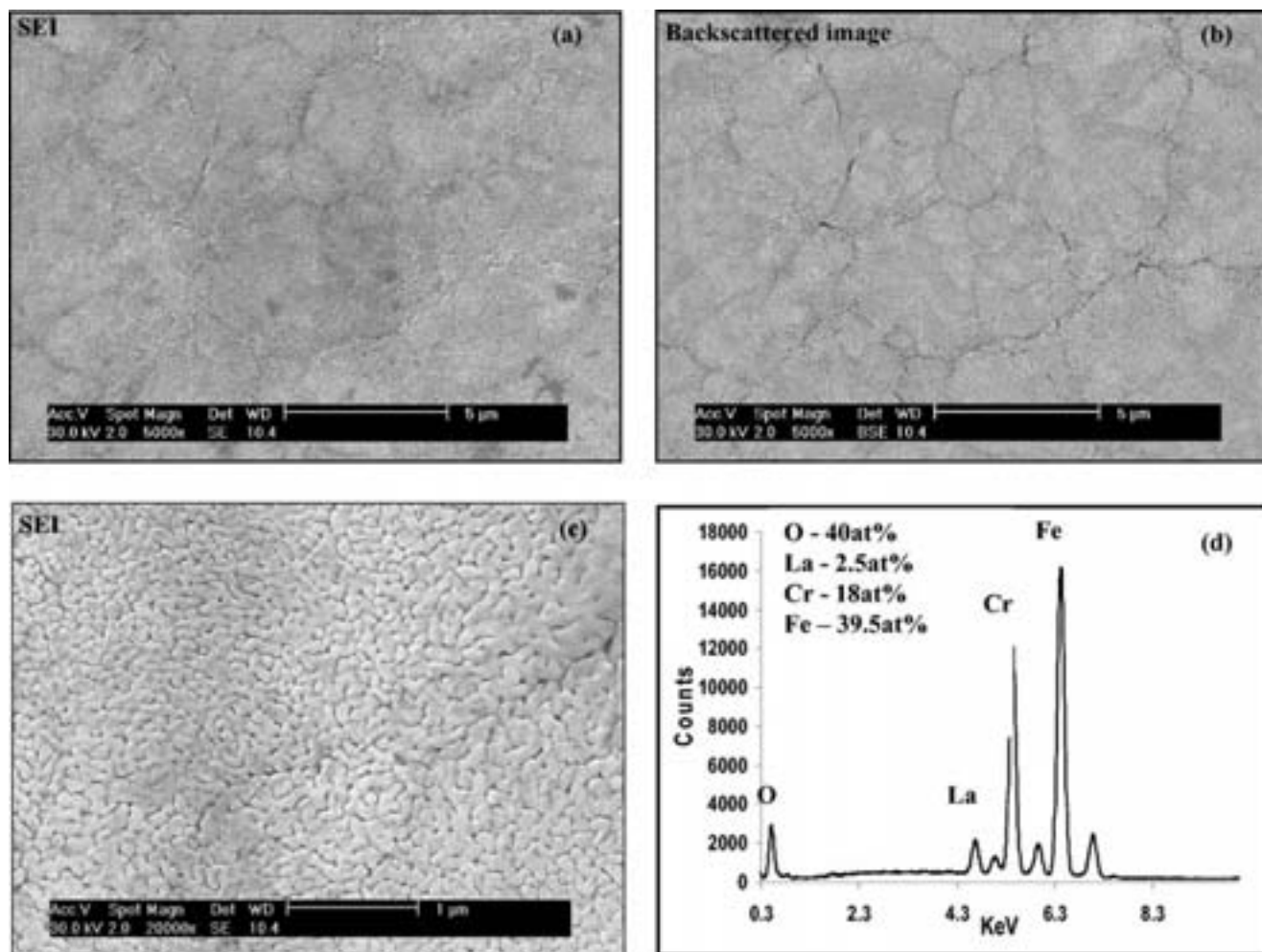


Fig. 2. LaCrO_3 perovskite surface after annealing at 700°C for 1 h: (a) and (c) SEI; (b) backscattered image; and (d) EDS analysis of the film.

Several structural features appear in SEM images of samples heated to 700°C for 1 h in air (Figs. 2(a)–(c)). Although few chromium-rich regions are detected on the film surface after annealing, the amount of chromium enrichment is substantially decreased in comparison with as-deposited film. Another structural feature clearly shown in the micrographs is large cracks that reveal the SS surface to the environment (Figs. 2(a) and (b)). The crack formation is likely the result of shrinkage during crystallization of the amorphous film. The mismatch in CTE between the film and substrate also may contribute to the crack formation. The CTE of SS is $10 \times 10^{-6} \text{ K}^{-1}$ and the CTE of LaCrO_3 is $9 \times 10^{-6} \text{ K}^{-1}$;¹¹ this results in the development of compressive residual stresses in the film during the cooling process. Yet another feature evident from the SEM micrographs is the fine dendrite structure that forms during annealing (Fig. 2(c)). This structure is especially pronounced at the grain boundaries; the largest dendrites are 300 nm long. The film inside the grains consists of small dendrites that tend to be organized in a self-assembled structure on the surface. The mechanisms of the dendritic self-assembled structure formation are described elsewhere.²⁰ The oxygen content in the annealed film is much higher as a result of annealing in air (Fig. 2(d)).

(2) X-ray Diffractometry and Raman Spectroscopy

The as-deposited sputtered thin film is amorphous, as indicated using XRD analysis. However, the amorphous film is Raman active, and, therefore, its vibration patterns have been studied using Raman spectroscopy. Typical Raman spectra of as-deposited LaCrO_3 thin film and a SS substrate are shown in Figs. 3(a) and (b). Three bands at 322, 731.6, and 1430.7 cm^{-1} (Table I) are

associated with the amorphous La-Cr-O structure (Fig. 3(a)), and, as expected, no bands are observed for SS (Fig. 3(b)).

To determine when and how perovskite structure development occurs, the same amorphous films were annealed in air at 300°C , annealed in air at 500°C for 15 min, and then annealed in air at 700°C for 1 h. XRD and Raman spectra were taken from the film surface after each annealing. The results are shown in Fig. 4. No peaks that belong to a crystalline structure are detected using XRD of the as-deposited film and films annealed at 300° and 500°C for 15 min. The well-developed LaCrO_3 perovskite structure is detected on the film surface annealed at 700°C for 1 h (Fig. 4(a)). No preferred orientation is detected, and, therefore, the film structure is isotropic. The calculated crystallite size of the LaCrO_3 thin film using the Scherrer equation²¹ is 218 Å.

Although XRD allows only study of the average structure of the film, micro-Raman spectroscopy can provide information about local microstructural developments as a result of annealing. Figure 4(b) shows that there are almost no changes in Raman spectra of the as-deposited film and the film annealed at 300°C . However, the film annealed at 500°C for 15 min has several weak bands in the $150\text{--}180 \text{ cm}^{-1}$ region, a diffuse broad band at 350 cm^{-1} , and a strong band at 856 cm^{-1} . The 856 cm^{-1} band also is present in the as-deposited film and films annealed at 300°C ; however, the band intensity is not as strong as after the 500°C annealing, and it strongly overlaps with another band at 730 cm^{-1} . The bands in the region $150\text{--}200 \text{ cm}^{-1}$ are tentatively assigned to rare-earth internal vibrations with respect to the Cr–O vibrations, the band at 730 cm^{-1} might be indicative of the lower-oxidation-state Cr^{3+} compound (LaCrO_3), and another band at 856 cm^{-1} might be indicative of

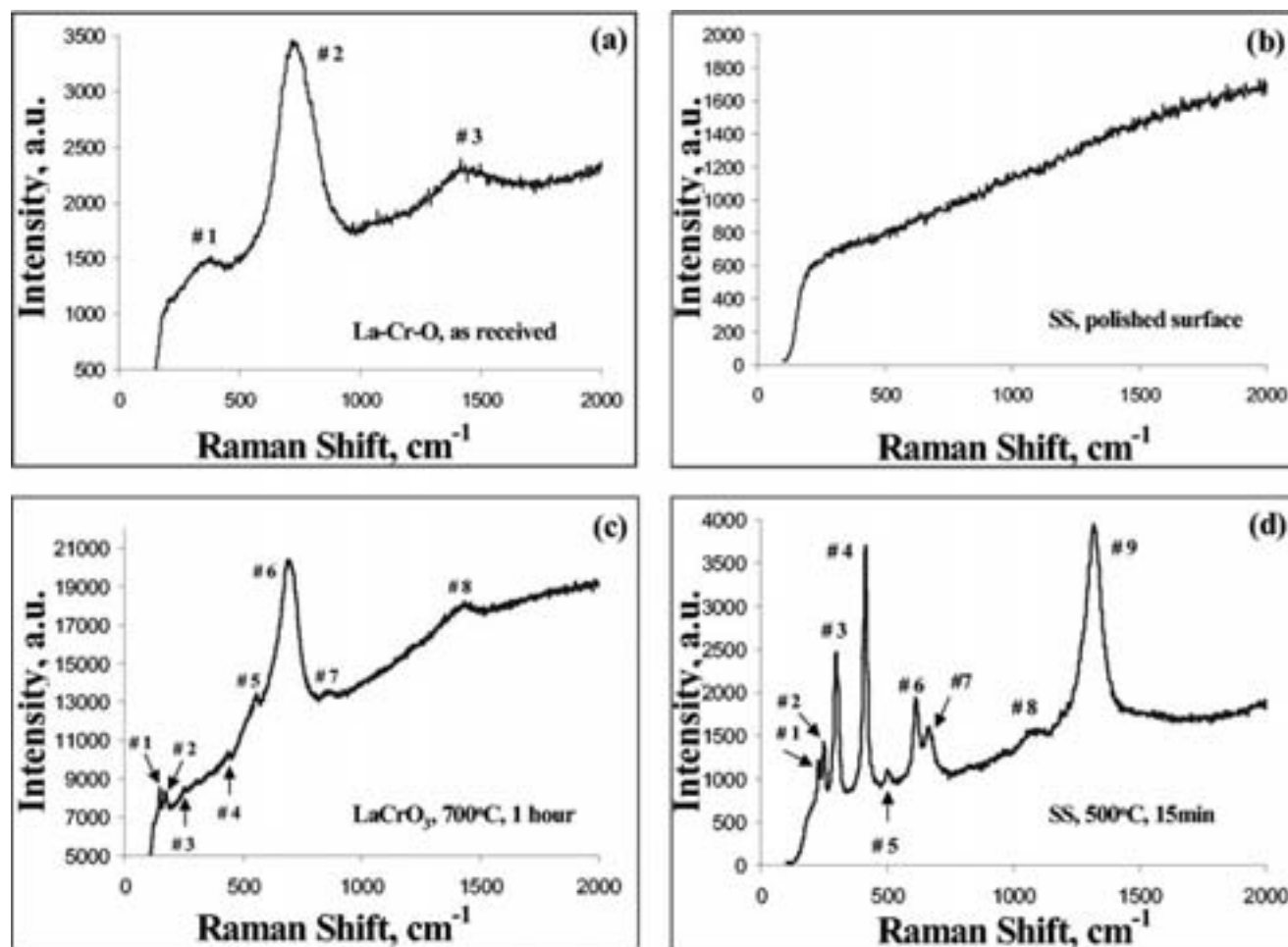


Fig. 3. Raman spectra taken from (a) an as-received surface after LaCrO_3 deposition using magnetron sputtering, (b) SS surface before LaCrO_3 deposition, (c) LaCrO_3 thin-film surface after annealing at 700°C for 1 h, and (d) SS surface after annealing at 500°C for 15 min.

the higher-oxidation-state Cr^{5+} (LaCrO_4).^{22,23} The band at 350 cm^{-1} always appears if the 856 cm^{-1} band is present. The intensity growth of the 856 cm^{-1} band during the annealing at 500°C is indicative of the beginning of the amorphous to LaCrO_4 monazite-type phase transition that occurs at $495^\circ\text{--}530^\circ\text{C}$.²⁰

When the films are further annealed at 700°C for 1 h, the Raman spectrum indicates the formation of perovskite structure (Fig. 4(b)). The low-energy part of the Raman vibrational spectrum is usually assigned to the vibrations that involve the motion of lanthanum relative to the MnO_6 octahedra, which is in accordance with the known classification of the phonon modes in cubic perovskite structure.²⁴ There are two lanthanum internal vibration bands at 149 and 172 cm^{-1} , several weak bands at 253 and 427 cm^{-1} , and two strong bands at ~ 581 and 695 cm^{-1} that are tentatively assigned to the O–Cr–O bending and stretching vibrations (Figs. 3(c) and 4(b)). At the same time, some residue of the 856 cm^{-1} band also is seen in this Raman spectrum. It may be possible that the intensity ratio of

the 695 and 856 cm^{-1} bands can be used to quantify the amount of various phases ($\text{LaCr}^{3+}\text{O}_3$ and $\text{LaCr}^{5+}\text{O}_4$) in the films as a function of annealing temperature. Band parameters, such as band position, height, full width at half maximum (FWHM), and band area are presented in Table II. Although a complete lattice dynamic calculation of the La–Cr–O systems is necessary for an unambiguous assignment of the Raman spectra, the main features observed in the present experiment are consistent with the published spectra of similar compounds.^{25–27}

The purpose of the film deposited on the SS surface is the protection of the SS surface against oxidation during SOFC operation. We have used Raman spectroscopy as a method to study such protection. There are a variety of phases formed on the SS surface without the protective LaCrO_3 film during annealing at 500°C for 15 min. The major oxide phase formed on the SS surface is hematite, $\alpha\text{-Fe}_2\text{O}_3$ (Fig. 3(d)), which has bands at 229.4 , 248.21 , 297.59 , 412.68 , 500.06 , 1088.7 , and 1316.54 cm^{-1} . The presence of the magnetite Fe_3O_4 band at 664 cm^{-1} also has been confirmed using this method. One band at 613 cm^{-1} has not been assigned to a compound, and neither chromite ($\text{Fe}^{2+}\text{Cr}_2\text{O}_4$) nor escholaite (Cr_2O_3) bands can be found on the SS surface. Band parameters obtained from the SS surface after annealing are presented in Table III. This result, when compared with when there is a LaCrO_3 perovskite coating on SS surface and only perovskite bands can be detected (Fig. 3(c)), suggests that the film is indeed acting to protect the SS substrate. Because the perovskite film thickness is $0.2\text{ }\mu\text{m}$, any subsurface oxide phase that forms is easily detected using Raman spectroscopy, which has at least $1\text{--}2\text{ }\mu\text{m}$ depth of penetration for a 514.5 nm laser.

Table I. Band Parameters of As-Received La–Cr–O Film Surface

Peak	Parameter (cm^{-1})			Area
	Center	Height	Width	
1	321.9	317	237	78908
2	731.6	1985	179	441146
3	1430.7	417	372	226829

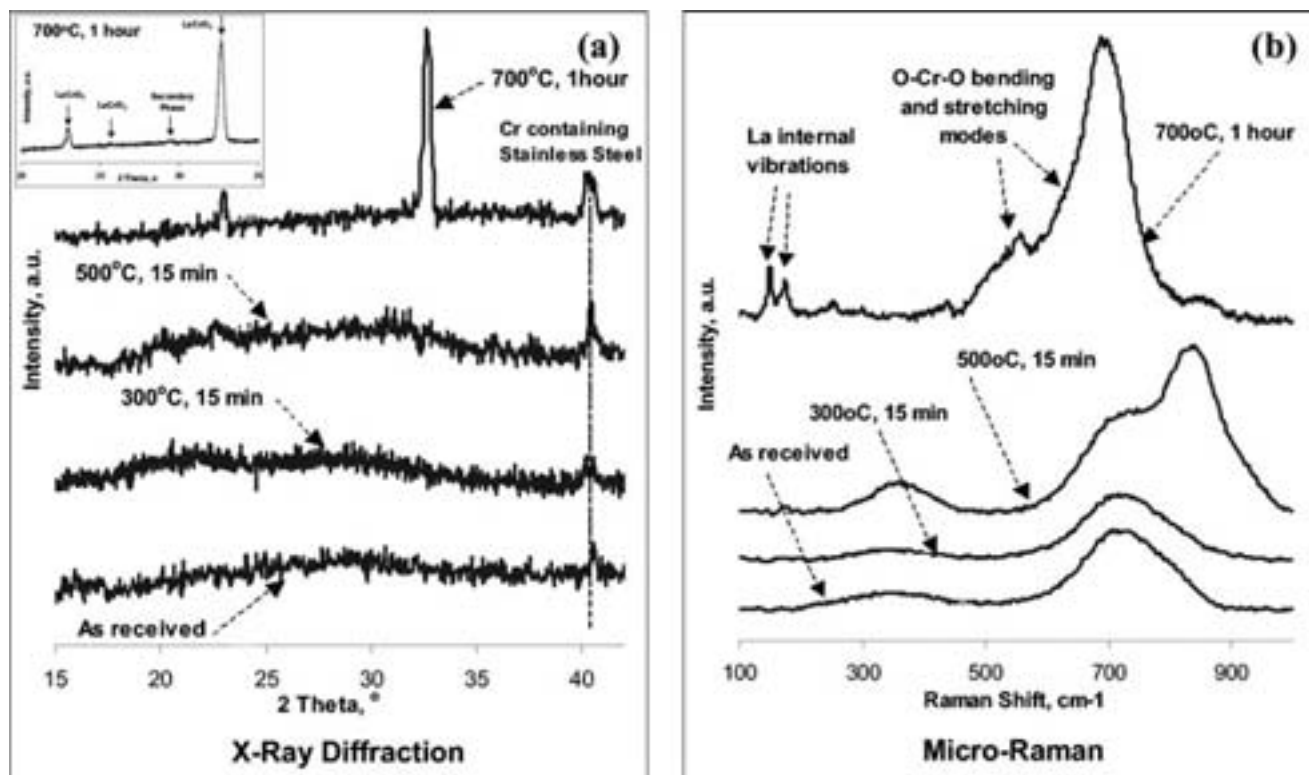


Fig. 4. (a) XRD pattern of LaCrO_3 coating annealed at various temperatures. Perovskite structure was formed after annealing at 700°C . Insert shows detailed XRD pattern of perovskite structure of the film annealed at 700°C for 1 h. (b) Raman spectra of LaCrO_3 coating annealed at various temperatures.

(3) Mechanical Response under Contact Loading

To properly design the cell elements, the knowledge of the mechanical properties of the materials is important. Nanoindentation allows estimation of the mechanical behavior of thin films. Deformation behavior, hardness, and Young's modulus of the as-deposited amorphous film were measured. The complete deformation behavior and mechanical properties of La-Cr-O_3 perovskite film after annealing are reported elsewhere.²⁸ To study the deformation behavior, the amorphous La-Cr-O film was indented with various displacements of the indenter to obtain 25%, 50%, and 100% penetration depth of the film thickness. Several indentations were done up to 300 nm displacement to penetrate the SS substrate. The nanoindentation also was performed on the polished SS surface without the La-Cr-O film; Young's modulus and hardness of SS were measured as 220.2 GPa and 2.5 GPa, respectively. The four typical load-displacement curves at various maximum loads are shown in Fig. 5. In all cases, the unloading curves do not overlap with loading curves, because irreversible plastic deformation takes place that leads to the formation of the residual impression on the material surface and, as a result, nonzero displacement when the load is removed after the test. There is

a deviation from expected $P \approx h^2$ behavior during loading at small loads up to ~ 2 mN.^{29,30} This is explained by (i) pure elastic response at the beginning of loading because the Berkovich indenter tip has some finite radius that affects the quadratic relationship with contact depth and (ii) the difference in the film structure and its stress state, where the indenter approaches the interface and the influence of SS substrate becomes significant.³¹ When the indenter penetrates the film at 25% of the film thickness, the measured values of hardness and Young's modulus were 9.37 GPa and 166.6 GPa, respectively. Hardness and Young's modulus were calculated from the beginning of each of the unloading curves, and hardness had a tendency to decrease and Young's modulus to increase as load-displacement increased. Such behavior is a result of the significant effect of the SS substrate, where the measured properties are properties of a film-substrate composite material.

IV. Summary

Thin-film LaCrO_3 was deposited using rf magnetron sputtering on SS 446 as a protective coating for this candidate SOFC

Table II. Band Parameters of LaCrO_3 Annealed at 700°C for 1 h

Peak	Parameter (cm^{-1})			Area
	Center	Height	Width	
1	149.3	1478	8.9	20113
2	172.7	922	13.9	14833
3	252.7	335	15	7936
4	426.6	130	13	2644
5	581.5	2167	159	367096
6	695.3	7820	87.5	795503
7	856.6	246	34	8896
8	1404.8	936	145.9	166463

Table III. Band Parameters Obtained from the Stainless-Steel Surface after Annealing at 500°C for 15 min

Peak	Parameter (cm^{-1})			
	Center	Height	Width	Area
1	229.4	234	14	
2	248.2	400	15	
3	297.6	1568	21.5	36138
4	412.7	2791	19	68135
5	500.1			
6	613.4	867	27	29967
7	664.3	502	48.5	25949
8	1088.7			
9	1316.5	2417	83	309077

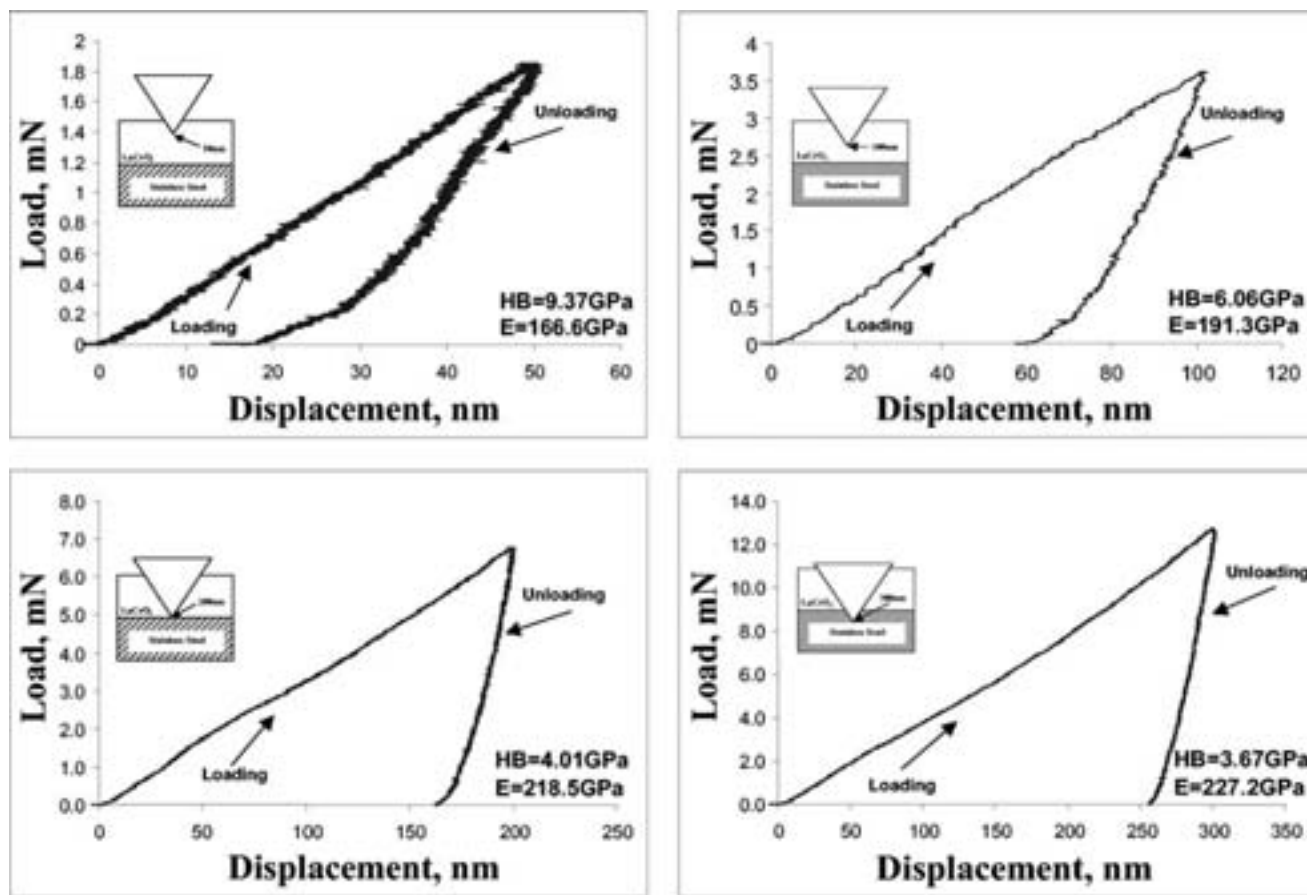


Fig. 5. Depth-controlling nanoindentation of as-received La-Cr-O thin film.

interconnect material. The thin film was amorphous in the as-deposited state, and it was crystallized after it was annealed in air. The surface of the as-deposited film was smooth and flat, whereas, after the film was annealed at 700°C, a self-assembled dendritic structure was developed.

The structure of the thin film was studied using XRD and micro-Raman spectroscopy. The XRD data indicated the perovskite crystal structure was well developed after it was annealed at 700°C. Use of micro-Raman spectroscopy allowed for the study of various stages of LaCrO_3 structure formation on a local scale. During these stages, the formation of an intermediate LaCrO_4 phase took place.

Comparison of the Raman spectra of the coated and uncoated substrates after annealing at 700°C showed that the uncoated substrate formed hematite ($\alpha\text{-Fe}_2\text{O}_3$) and magnetite (Fe_3O_4), whereas the coated SS 446 surface showed only LaCrO_3 . Because the penetration depth of the laser was deeper than the thickness of the film, the lack of hematite and magnetite formation was attributed to protection from the LaCrO_3 layer. The annealing thus far was at relatively low temperatures (700°C) and short times (1 h); nonetheless, it indicated that Raman spectroscopy could be used in reasonably thin films (<1–2 μm) to determine the effectiveness of Raman-active protective coatings.

Preliminary mechanical properties, measured using nanoindentation, were reported for the amorphous as-deposited film. The hardness and Young's modulus of the amorphous film were measured to be 9.37 GPa and 166.6 GPa, respectively.

Future work will include studying the film stability after long-term annealing experiments at 700°–800°C, measuring the area specific resistance of the films, and completing the mechanical evaluation of the films. We anticipate using the information gained here to determine what properties of the perovskite film need to be optimized, and then will either dope the LaCrO_3

material to meet these property needs or choose an alternative perovskite that is better suited for the purpose.

References

- ¹W. Z. Zhu and S. C. Deevi, "Development of Interconnect Materials for Solid Oxide Fuel Cells," *Mater. Sci. Eng. A*, **348** [1–2] 227–43 (2003).
- ²K. Huang, J. Wan, and J. B. Goodenough, "Oxide-Ion-Conducting Ceramics for Solid Oxide Fuel Cells," *J. Mater. Sci.*, **36** [5] 1093–98 (2001).
- ³K. Huang, P. Y. Hou, and J. B. Goodenough, "Characterization of Iron-Based Alloy Interconnects for Reduced Temperature Solid Oxide Fuel Cells," *Solid State Ionics*, **129** [1–4] 237 (2000).
- ⁴P. Y. Hou and J. Stringer, "The Effect of Reactive Element Additions on the Selective Oxidation, Growth, and Adhesion of Chromia Scales," *Mater. Sci. Eng. A*, **202** [1–2] 1–10 (1995).
- ⁵S. Chevalier and J. P. Larpin, "Formation of Perovskite-Type Phases during the High-Temperature Oxidation of Stainless Steels Coated with Reactive Element Oxides," *Acta Mater.*, **50** [12] 3105–14 (2002).
- ⁶J. S. Park and H. G. Kim, "Electrical Conductivity and Defect Models of MgO-Doped Cr_2O_3 ," *J. Am. Ceram. Soc.*, **71** [4] 173–76 (1988).
- ⁷A. Paul, J. A. Odriozola, M. A. San Miguel, J. Fernandez Sanz, and L. J. Alvarez, "Experimental and Molecular Dynamics Simulation Analysis of LaCrO_3 Precipitation in Chromia Scales," *Acta Mater.*, **48** [11] 2951–58 (2000).
- ⁸W. J. Quaddakers, H. Greiner, M. Hansel, A. Pattanaik, A. S. Khanna, and W. Mallener, "Compatibility of Perovskite Contact Layers between Cathode and Metallic Interconnector Plates of SOFCs," *Solid State Ionics*, **91** [1–2] 55–67 (1996).
- ⁹S. Linderth, "Controlled Reactions between Chromia and Coating on Alloy Surface," *Surf. Coat. Technol.*, **80** [1–2] 185–89 (1996).
- ¹⁰S. Sehlin, H. Anderson, and D. Sparlin, "Electrical Characterization of the (La,Ca)(Cr,Co)O₃ System," *Solid State Ionics*, **78** [3–4] 235–43 (1995).
- ¹¹E. Suda, B. Pacaud, T. Seguelong, and Y. Takeda, "Sintering Characteristics and Thermal Expansion Behavior of Li-Doped Lanthanum Chromite Perovskites Depending Upon Preparation Method and Sr Doping," *Solid State Ionics*, **151** [1–4] 335–41 (2002).
- ¹²M. Rajendran, M. G. Krishna, and A. K. Bhattacharya, "Low-Temperature Preparation of Orthoferrite Thin Films by Inorganic Sol–Gel Process," *Thin Solid Films*, **385** [1–2] 230–33 (2001).
- ¹³W. Wu, K. H. Wong, and C. L. Choy, "A Comparative Study of *In Situ* Annealing Effects on the Electrical Transport Behavior of Epitaxial $\text{La}_{0.5}\text{Sr}_{0.5}\text{CoO}_3$ and $\text{La}_{0.7}\text{Sr}_{0.3}\text{MnO}_3$ Thin Films," *Thin Solid Films*, **385** [1–2] 298–301 (2001).

- ¹⁴M. J. Montenegro, T. Lippert, S. Mueller, A. Weidenkaff, P. R. Willmott, and A. Wokaun, "Pulsed Laser Deposition of Electrochemically Active Perovskite Films," *Appl. Surf. Sci.*, **197-198**, 505-11 (2002).
- ¹⁵I. Taniguchi, R. Van Landschoot, and J. Schoonman, "Fabrication of La_{1-x}Sr_xCo_{1-y}Fe_yO₃ Thin Films by Electrostatic Spray Deposition," *Solid State Ionics*, **156** [1-2] 1-13 (2003).
- ¹⁶K. Wasa, Y. Haneda, T. Satoh, H. Adachi, and K. Setsune, "Sputtering Deposition of Perovskite Thin Films with Atomic-Scale Controlled Surface," *Appl. Surf. Sci.*, **121/122**, 152-55 (1997).
- ¹⁷D. O. Klenov, W. Donner, L. Chen, A. J. Jacobson, and S. Stemmer, "Composition Control of Radio-Frequency Magnetron Sputter-Deposited La_{0.5}Sr_{0.5}CoO_{3-δ} Thin Films," *J. Mater. Res.*, **18** [1] 188-94 (2003).
- ¹⁸L. L. Hay and G. Pharr, "Instrumented Indentation Testing"; pp. 231-40 in *Mechanical Testing and Evaluation*, Vol. 8-03D. Edited by H. Kuhn and D. Medlin. ASM International, Materials Park, OH, 2000.
- ¹⁹M. Martin and M. Troyon, "Fundamental Relations Used in Nanoindentation: Critical Examination Based on Experimental Measurements," *J. Mater. Res.*, **17** [9] 2227-34 (2002).
- ²⁰C. Johnson, R. Gemmen, and N. Orlovskaya, "Nanostructured Self-Assembled LaCrO₃ Thin Film Deposited by RF Magnetron Sputtering on a Stainless Steel Interconnect Material," *Compos., Part B: Eng.*, **35** [2] 167-72 (2004).
- ²¹H. Araki, "Micro Area X-ray Diffraction Techniques," *Rigaku J.*, **6** [2] 34-42 (1989).
- ²²D. H. Cho, S. D. Yim, G. H. Cha, J. S. Lee, Y. G. Kim, J. S. Chung, and I.-S. Nam, "Behavior of Chromium Oxide on MgO or MgF₂," *J. Phys. Chem. A*, **102** [41] 7913-18 (1998).
- ²³K. Azegami, M. Yoshinaka, K. Hirota, and O. Yamaguchi, "Formation and Sintering of LaCrO₃ Prepared by the Hydrazine Method," *Mater. Res. Bull.*, **33** [2] 341-48 (1998).
- ²⁴K. H. Kim, J. Y. Gu, H. S. Choi, and G. W. Park, "Frequency Shifts of the Internal Phonon Modes in La_{0.7}Ca_{0.3}MnO₃," *Phys. Rev. Lett.*, **77** [9] 1877-80 (1996).
- ²⁵M. Popa, L. V. Hong, and M. Kakihana, "Nanopowders of LaMeO₃ Perovskites Obtained by a Solution-Based Ceramic Processing Technique," *Physica B*, **327**, 233-36 (2003).
- ²⁶Y. Aoki, H. Konno, H. Tachikawa, and M. Inagaki, "Characterization of LaCrO₄ and NdCrO₄ by XRD, Raman Spectroscopy, and ab Initio Molecular Orbital Calculations," *Bull. Chem. Soc. Jpn.*, **73**, 1197-203 (2000).
- ²⁷V. B. Podobedov, A. Weber, D. B. Romero, J. P. Rice, and H. D. Drew, "Raman Scattering in La_{1-x}Sr_xMnO₃ Single Crystals (x = 0, 0.1, 0.2, 0.3)," *Solid State Commun.*, **105** [9] 589-93 (1998).
- ²⁸A. Coratolo, N. Orlovskaya, M. Lugovy, V. Sljunyaev, S. Dub, C. Johnson, and R. Gemmen, "Nanoindentation of LaCrO₃ Thin Film," *J. Mater. Sci.*, in review.
- ²⁹K. Zeng, S. Soderlund, A. Giannakopoulos, and D. Rowcliffe, "Controlled Indentation: A General Approach to Determine Mechanical Properties of Brittle Materials," *Acta Mater.*, **44** [3] 1127-41 (1996).
- ³⁰W. Oliver and G. Pharr, "An Improved Technique for Determining Hardness and Elastic Modulus Using Load and Displacement Sensing Indentation Experiments," *J. Mater. Res.*, **7** [6] 1564-83 (1992).
- ³¹T. Tsui, J. Vlassak, and W. Nix, "Indentation Plastic Displacement Field: Part I. The Case of Soft Films on Hard Substrates," *J. Mater. Res.*, **14** [6] 2196-203 (1999). □